scientific reports

Check for updates

OPEN

MT1H inhibits the growth of gastric cancer by regulating SLC6A19/TTC39B/ADM2 and activating p53-dependent autophagy

Yamin Xing[1,2,5], Guangyuan Li[1,2,5], Ganggang Li[2], Jixuan Xu[3], Ting Zhang[2], Mengxue Li[1], Chunxiao Gao[1,2], Miaoran Fu[4], Pengyuan Zheng[1]✉ & Xiufeng Chu[1,2]✉

Metallothioneins (MTs) are a class of cysteine-rich proteins that actively participate in the cellular defense against free radicals. However, owing to the high heterogeneity among different MTs, comprehensive investigations are needed to determine the biological activities and distribution patterns of each MT in different tissues. In the present study, ectopic expression of MT1H significantly inhibited the proliferation of gastric cancer cells. Mechanistically, MT1H was transported into the nucleus and regulated the expression of key genes involved in nutrient transportation and homeostasis, such as SLC6A19, TTC39B, and ADM2, and thereby activating the p53 and autophagy pathways. Additionally, survival analysis of data from the TCGA and other databases revealed that gastric cancer patients with high expression of MT1H had longer survival. Furthermore, MT1H was undetectable in most gastric cell lines, but its expression was increased upon treatment with dexamethasone (Dexa) and the metal ion zinc. Therefore, MT1H emerges as a valuable tumor suppressor, a biomarker for the prognosis, and a promising therapeutic target in gastric cancer patients.

Keywords Metallothionein, Gastric cancer, p53, Autophagy

MTs are a class of cysteine-rich proteins that bind various metal ions[1]. They not only enhance the cellular defense against free radicals but also participate in metal ion-related events, ranging from detoxification to homeostasis, storage, and transfer of metal ions[2,3]. MTs consist of four major subtypes: MT1, MT2, MT3, and MT4[4]. MT1 and MT2 are ubiquitously expressed across tissues in response to excessive metal ions and oxidative stress[6]. In contrast, MT3 is constitutively expressed in the central nervous system[2,7], and MT4 is prominently expressed in proliferative stratified epithelial tissues[8]. Notably, the primate MT1 family comprises 13 unique isoforms (MT1A to MT1J, MT1L, MT1M, and MT1X), which introduce significant complexity in delineating the biological roles of individual MT isoforms in humans[9].

Increasing evidence shows that MTs play a pivotal role in tumor formation, progression, and drug resistance by regulating apoptosis, proliferation, angiogenesis, and the detoxification of heavy metals[4,10,11]. Furthermore, MTs are not universally expressed in human tumors but dependent on various factors, such as tumor type, stage, or cellular origin[12]. For example, MT1G inhibits the growth of thyroid tumors by regulating the PI3K/Akt and Rb/E2F pathways[13,14]. MT1H is downregulated and associated with poor outcomes in prostate cancer patients[15]. In our current study, we found that MT1H suppresses tumor growth via p53 cell cycle arrest in gastric cancer. Mechanistically, MT1H affected the expression of key genes in nutrient homeostasis and resulted in the activation of p53-dependent autophagy pathways. In the patients with gastric cancer, high-MT1H is correlated with a longer survival time. But MT1H was generally downregulated in tumor tissue when compared to normal tissue. Interestingly, treatment with Dexa and zinc significantly induced the expression of MT1H in gastric cancer cells, thus giving a clue for the combination of MT1H inducers and the anti-tumor agents that are conventionally used in clinical practice.

[1]Marshall B. J. Medical Research Center, Zhengzhou University, Zhengzhou 450052, Henan, China. [2]Department of Oncology, The Fifth Affiliated Hospital of Zhengzhou University, Zhengzhou, China. [3]Department of Gastrointestinal & Thyroid Surgery, The Fifth Affiliated Hospital of Zhengzhou University, Zhengzhou, China. [4]Department of Neurology, The Fifth Affiliated Hospital of Zhengzhou University, Zhengzhou, China. [5]Yamin Xing and Guangyuan Li contributed equally to the work. ✉email: pyzheng@zzu.edu.cn; Chuxiufeng831031@gmail.com

Results

MT1H is a unique primate metallothionein

MT1H is one of the arrayed duplicate MT1 genes[9] and exists only in primates but not in other organisms. In humans, the MT1H gene is located on chromosome 16 and encodes a small protein of 61 amino acids, which contains a high content of cystines (Fig. 1A-C). Structural analysis revealed that MT1H is evolutionarily conserved, and its amino acid sequence is highly similar to that of other MT1s (Fig. 1D, E). Based on these findings, we speculated that MT1H has basic functions similar to those of other MTs, such as metal binding and antioxidant activity, and that MT1H participates in additional distinct biological processes due to peptide sequence variation.

MT1H is a tumor suppressor in gastric cancer

SGC-7901 and ASG, derived from gastric adenocarcinoma patients, are two cell lines widely used to study the biological behaviors and signaling pathways of gastric cancer, such as tumorigenesis, metastasis, and chemoresistance. To test whether MT1H affects the viability of gastric cancer cells, we created SGC-7901-tetO-MT1H-OV and AGS-tetO-MT1H-OV cells and thus achieved a doxycycline (Dox)-induced expression of MT1H (Fig. 2A, B). We found MT1H caused a significant decrease of cell number coupled with morphological changes (Fig. 2C). Consistently, ATP-based Cell Titer and dehydrogenase-based CCK-8 assays revealed a declined viability in MT1H-expressing cells (Fig. 2D, E). In mice, SGC-7901 xenografts overexpressing MT1H exhibited a significant reduction in tumor growth (Fig. 2F-I). Next, we analyzed the cell cycle and apoptosis via flow cytometry to determine the biological processes affected by MT1H. We found that MT1H caused a reduction in the number of cells in the S/G2 phase and subsequent cell cycle arrest (Fig. 3A). No changes in apoptosis were observed between MT1H-overexpressing cells and control cells (Fig. 3B). These findings suggest that MT1H suppresses tumor growth via cell cycle arrest. We next aimed to elucidate the underlying mechanisms behind the tumor suppressor function of MT1H in gastric cancer.

Functional enrichment analysis of differentially expressed genes in MT1H-overexpressing cells

Transcriptionally regulating survival signaling is an important mechanism through which tumor suppressors exert their functions, such as p53[16], Rb[17]. Interestingly, our subcellular fractionation assay revealed the localization of MT1H in both the cytoplasm and nucleus (Fig. 4A), a feature of transcription factors[18–22]. Together with the knowledge that the transcription factor activity is generally subject to the accessibility of the metal ion zinc[23–26], we hypothesized that the metal-binding protein MT1H directly or indirectly regulates gene transcription. To determine this, a transcriptome analysis was performed in SGC-7901-tetO-MT1H-OV cells via bulk mRNA sequencing (RNA-Seq) (Fig. 4B). We identified 517 differentially expressed genes caused by MT1H overexpression (MT1H-DEGs) (Fig. 4C). First, MT1H-DEGs were shown in volcano plot and heat map, where the top ten upregulated and downregulated of them were annotated to decipher MT's anti-tumor function. (Fig. 4D, E, and Suppl. Extended Table 1). Next, functional enrichment analyses were performed to further understand the functions of the MT1H-DEGs. COG function classification revealed that MT1H-DEGs were enriched in "Signal transduction mechanisms", "Posttranslational modification, protein turnover, chaperones", "Amino acid transport and metabolism", "Inorganic ion transport and metabolism", and "Lipid transport and metabolism" (Fig. 5A). KEGG indicated that MT1H-DEGs were enriched mainly in cancer-related pathways, particularly the PI3K-Akt signaling pathway (Fig. 5B, C). In GO enrichment analysis, MT1H-DEGs were significantly enriched in the terms "Response to hypoxia", "metal ion binding" and "sarcomere" (Fig. 5D-F). These data suggest that MT1H plays a role in the regulation of energy metabolism, metal ion transport, and muscle movement.

MT1H activates p53-dependent autophagy

Among these MT1H-DEGs, just a few of them were highly regulated by MT1H, the expressions of which were changed more than two-fold by MT1H (Extended Table 1). We performed semiquantitative PCR (Semi-qPCR) to verify the top 4 downregulated and 4 upregulated MT1H-DEGs. The primers were designed to span introns to avoid interference from genome DNA (Extended Table 2). Agarose Gel analysis of semi-qPCR products revealed that SLC6A19 was downregulated and TUBB2B/TTC39B/ADM2/ATP1B2 were upregulated in MT1H-overexpressing cells (Fig. 6A). Next, information about these genes was collected from multiple sources, including UniProt, Protein Atlas, InterPro, GeneCards, STRING (v12.0), NCBI as well as the PubMed literature. SLC6A19 is a transmembrane protein that actively transports most neutral amino acids across the apical membrane of renal and intestinal epithelial cells in a sodium-dependent and chloride-independent manner[27,28]. By regulating amino acid availability, SLC6A19 could influence the activation of mTORC1 and autophagy[29,30]. TTC39B maintains cellular homeostasis via lipid-induced autophagy. Mechanistically, TTC39B promotes the ubiquitination and degradation of the oxysterol receptors LXR, the activation of which is associated with lipid metabolism and autophagic regulation, especially in the context of lipid or mitochondrial stress[31]. ADM2 is a member of the calcitonin gene-related peptide (CGRP)/calcitonin family of hormones that play a role in the regulation of food-water intake[32]. Mechanistically, ADM2 could regulate autophagic processes by activating the cAMP-dependent pathway or promoting the ubiquitination and degradation of LXR receptors[32] under stress conditions, such as oxidative stress or nutrient deprivation[33,34]. Consistent with the crosstalk between nutrient signaling and autophagy[35,36], we found that overexpressing MT1H in cells upregulated p53 and LC3B (Fig. 6B). Together with the knowledge of the KEGG pathway (Fig. 6C), we concluded that MT1H regulates the transcription of nutrient-related genes and subsequently results in p53-dependent autophagy (Fig. 6D).

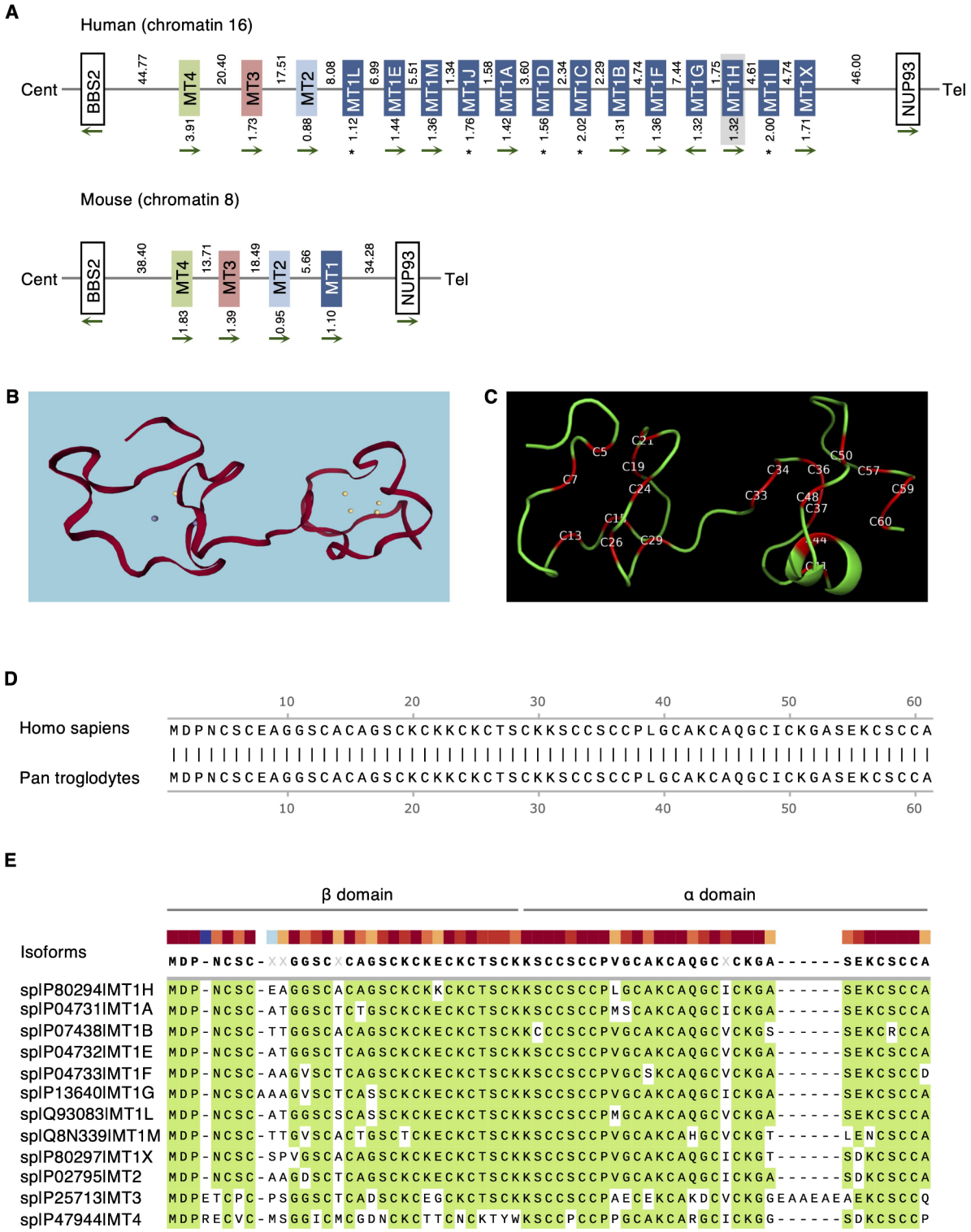

Fig. 1. MT1H is a unique member of the metallothionein family in primates. (A) Illustration of the MT family in human and mouse. In mice, the family comprises four functionally active genes (MT1 to MT4). In humans, MT1 family harbors a single-copy of MT2, MT3 and MT4, and a tandemly duplicated array of the MT1 duplicates spanning about 66.6 Kb. Among MT1 genes, the active gene is marked with an arrow showing transcription direction, and the inactive gene is indicated by an asterisk. Numbers corresponding to gene sizes and intergenic regions are given in Kb. (B) MT1H structure was predicted by SWISS-MODEL[56] (SMR, https://swissmodel.expasy.org). (C) MT1H structure was predicted by AlphaFold2[57] (https://alphafold.ebi.ac.uk) and represented using PyMOL software (Version 2.6.2, https://pymol.org). (D) MT1H among species was aligned using SnapGene-Smith-Waterman (Version 6.0.2). E, MT1H alignment among metallothionein family with SnapGene-MUSCLE (Version 6.0.2).

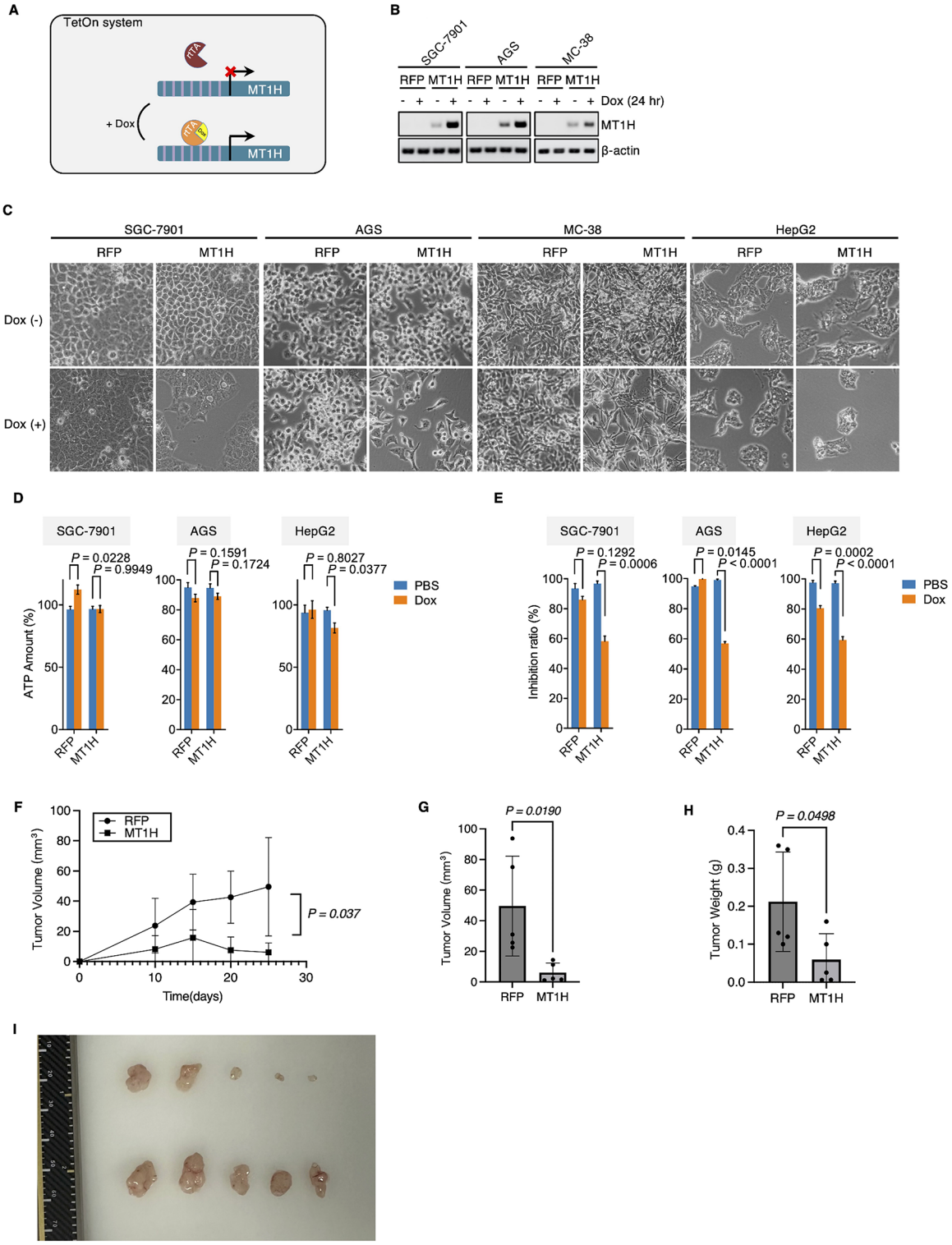

MT1H is a favorable biomarker for the prognosis of gastric cancer

Next, to assess the correlation between MT1H expression and survival in gastric cancer patients, we performed survival analysis via the online tool Kaplan-Meier (KM) plotter[37,38]. A total of 875 patients from GSE14210 ($n = 145$), GSE15459 ($n = 200$), GSE22377 ($n = 43$), GSE29272 ($n = 268$), GSE51105 ($n = 94$), and GSE62254 ($n = 300$) were included. The patients were split into two groups according to the median expression of MT1H. KM plot analysis revealed that patients in the MT1H-high group had a significantly longer median overall survival than those in the MT1H-low group (Fig. 7A). Interestingly, HER2 status affected the predictive efficiency of MT1H. The survival of patients in the HER2 (-) group, but not in the HER2 (+) group, was significantly associated with the expression of MT1H (Fig. 7B, C). Therefore, it is reasonable to conclude that MT1H is a favorable survival biomarker in HER2 (-) gastric cancer.

◀**Fig. 2**. MT1H suppresses tumorigenic activities of both gastric cancer and liver cancer cells. (A) Tetracycline on (TetOn) system uses tetracycline (or one of its analogs like doxycycline) as a regulator of gene expression. Tetracycline-dependent promoter is created by placing a TRE upstream of a minimal promoter. TRE is 7 repeats of tetracycline operator (tetO) sequence and is recognized by **r**everse **t**etracycline-controlled **trans**activator (rtTA). In the presence of tetracycline or one of its analogs like doxycycline (Dox), rtTA will bind to tetracycline and the TRE, permitting transcription. (B) Cells were transduced to express tetO-RFP or tetO-MT1H. To verify MT1H expression, cells were treated with Dox (2 μg/ml). 24 h later, cells were harvested and subjected to semi-qPCR assay. (C) Morphological changes by MT1H. Number of the cells expressing tetO-RFP or tetO-MT1H was measured, and 1×10^5 cells were seeded into 6-well plate. Dox (2 μg/ml) was added to induce the expression of RFP or MT1H. 7 days later, images were taken to observe cells` morphological changes. (D) 1×10^2 of the cells expressing tetO-RFP or tetO-MT1H were seeded into 96-well plate. 7 days after Dox treatment, cells were subjected to ATP-based cell viability assay. (E) Similar to (D), except that cells were subjected to CCK-8 assay. (F) Tumor growth curve was measured after subcutaneous injection of RFP and SGC7901-MT1H. The tumor volume was calculated every 5 days. The error line represents the standard deviation. (G) Comparison of tumor volume between SGC7901-RFP and SGC7901-MT1H implanted in mice on day 25. (H) Comparison of tumor weight between SGC7901-RFP and SGC7901-MT1H implanted in mice on day 25. (I) Photos of the dissected tumors from nude mice. In F-I, the error bar represents the standard deviation ($n = 5$).

MT1H is downregulated in gastric cancer and can be rescued by the treatment of Dexa and zinc

Dysregulation of MTs has been observed in many cancers, but each cancer exhibits a tissue-specific expression pattern[10,39–41]. To analyze MT1H expression in gastric cancer, we first searched the TNM plot platform and gathered patient data from the GEO, GTex, TCGA, and TARGET databases[42]. RNA-Seq analysis indicated that MT1H was downregulated in gastric cancer (Fig. 8A), which was further confirmed via data from gene chips (Fig. 8B). Moreover, both TNM plot and GEPIA[43] showed downregulation of MT1H in the cancers that are derived from other parts of the digestive system (Fig. 8C, D). Consistent with these findings, we found that the gastric cancer cell lines presented very low expression of MT1H (Fig. 9A, B).

To pharmaceutically restore MT1H expression in gastric cancer cells, we screened the literature and identified several candidate inducers of MT1H, including Dexa, cisplatin, zinc (Zn^{2+}), copper (Cu^{2+}) and iron (Fe^{2+}). Gastric cells were treated with these candidates and subjected to a semi-qPCR assay. We found that Dexa/Cisplatin/zinc significantly induced the expression of MT1H (Fig. 9C-E), whereas copper/iron had no or negligible effects on MT1H expression (Fig. 9F, G). These findings give us a clue that adjuvant treatment with glucocorticoids or zinc may suppress tumor growth by upregulating MT1H during conventional anti-cancer interventions.

Discussion

The digestive system is the primary site for mineral absorption[44]. Increasing evidence suggests the contribution of dysregulated nutrient signaling to the tumorigenesis of the digestive system[44,45]. MTs, first identified in the horse kidney in 1957[46], participate in metal metabolism, detoxification, and antioxidant processes through binding metal ions, such as zinc, copper, cadmium, etc[47]. The involvement of MTs in tumorigenesis is documented in various human cancers derived from the digestive system[4,10]. For example, Zheng et al. showed that MT1H suppresses the proliferation of hepatocellular cancer (HCC) cells by inhibiting the Wnt/β-catenin pathway[48]. Hung et al. demonstrated that the simultaneous downregulation of six MT1 genes occurs in colorectal cancer (CRC), and the four-gene signature (MT1F, MT1G, MT1L, and MT1X) can accurately predict clinical outcomes of CRC patients[49]. Liu et al. further revealed that MT2A suppresses CRC cell proliferation by inhibiting the Hippo signaling pathway[50]. In this study, we demonstrated that MT1H functioned as a tumor suppressor in gastric cancer cells. Mechanistically, MT1H translocated into the nucleus and modulated the expression of key genes involved in nutrient homeostasis, leading to the activation of p53-dependent autophagy and cell cycle arrest.

Given that MT1H is downregulated in gastric cancer, it is plausible that enhancing its expression could suppress tumor growth. We observed that dexamethasone (Dexa) and zinc robustly induced MT1H expression in gastric cancer cells. Consequently, the clinical application of glucocorticoids and zinc as adjuvant therapy may offer therapeutic benefits for gastric cancer patients. Of course, studies assessing the pharmacokinetics and toxicity profiles of MT1H-targeting drugs in preclinical animal models will be crucial before advancing to clinical trials. The role of MT1H in cisplatin-based chemotherapy, however, remains controversial. While cisplatin-induced MT1H could inhibit tumor growth via its tumor-suppressive activity, it may simultaneously bind and inactivate cisplatin through its metal-binding capacity, thereby potentiating cisplatin resistance in gastric cancer. To resolve this paradox, further studies using MT1H-knockout cells or MT1H-transgenic models are warranted[51,52]. Additional experiments are also needed to explore the combinatorial effects of MT1H inducers and conventional anti-tumor agents both in vitro and in vivo.

The discovery of novel biomarkers is one of the ideal destinations for medical study. Tumor-specific or tumor-related biomarkers themselves or combined with others provide promising direction, such as KMT2A-G3131S for familial myeloproliferative neoplasms[53], GNL3L for acute myeloid leukemia[54]. In our study, the median overall survival (mOS) of gastric cancer patients is positively correlated with MT1H expression, suggesting its potential as a biomarker for predicting patient outcomes. Nonetheless, MT1H is neither a secretory protein nor a membrane protein, and the high homology among MMT subtypes makes it challenging to produce MT1H-

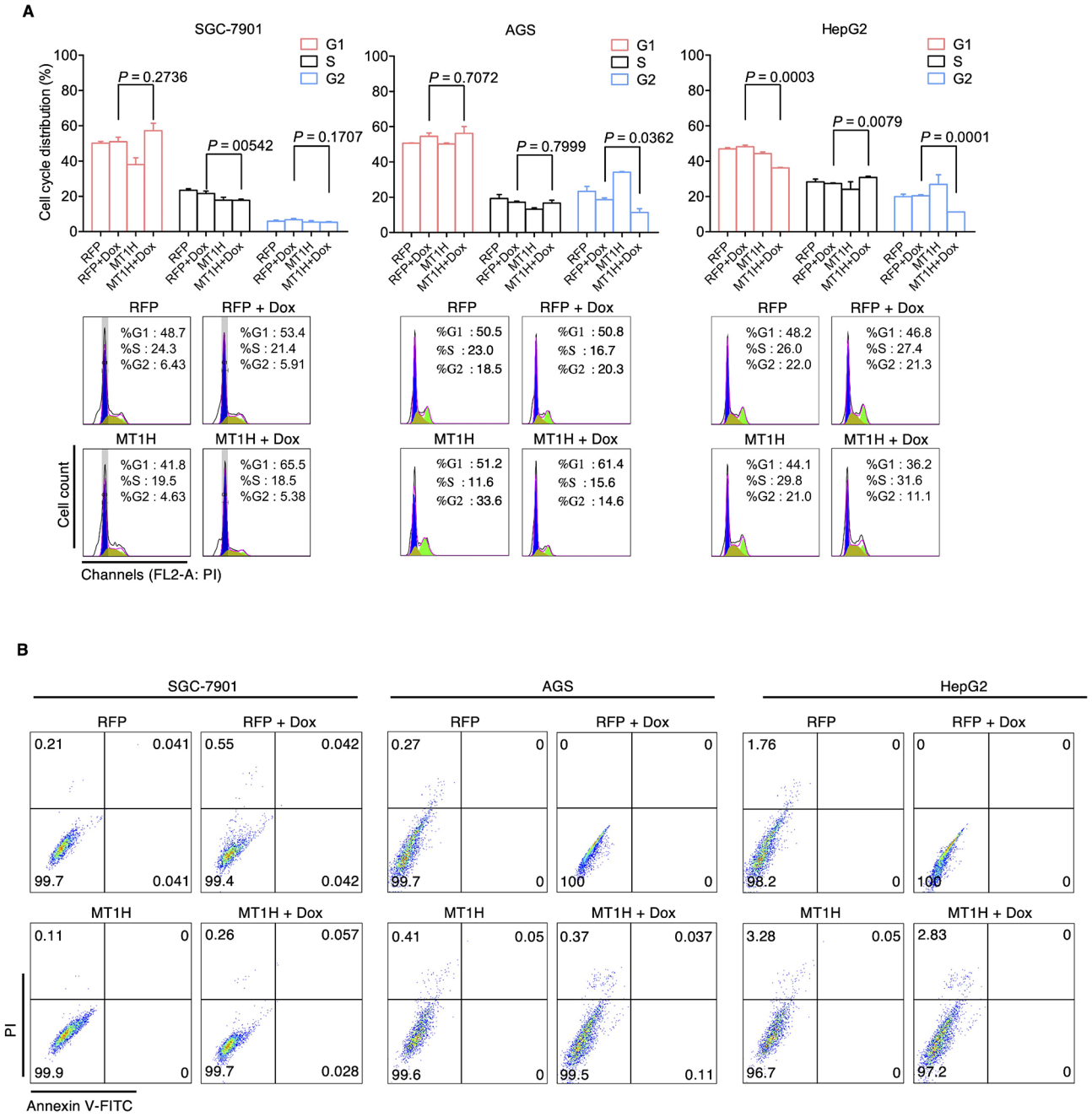

Fig. 3. MT1H induces cell cycle arrest in gastric cancer cells. (A) 1×10^5 cells were seeded into 6-well plate. Dox (2 μg/ml) was added to induce the expression of RFP or MT1H. 3 days after Dox treatment, the cells were subjected to cell cycle analysis. (B) 1×10^5 cells were seeded into 6-well plate. Dox (2 μg/ml) was added to induce the expression of RFP or MT1H. 3 days after Dox treatment, the cells were harvested and subjected to apoptosis analysis using Annexin V/PI double staining kit.

specific antibodies. Therefore, conventional methods, including flow cytometry, immunohistochemistry, and serological testing, are unsuitable for MT1H detection. Currently, the most feasible method is to detect the mRNA level of MT1H in tumor tissue through quantitative PCR or RNA-Seq. Besides, MT1H was downregulated not only in gastric cancer but also in cancers from other parts of the digestive system (shown in Fig. 8), making it difficult to determine the source of cancer cells merely based on MT1H expression. Therefore, integrating MT1H status with other biomarkers should always be considered. For example, RNA chips can be designed to combine MT1H and other novel biomarkers that cannot be detected through conventional methods.

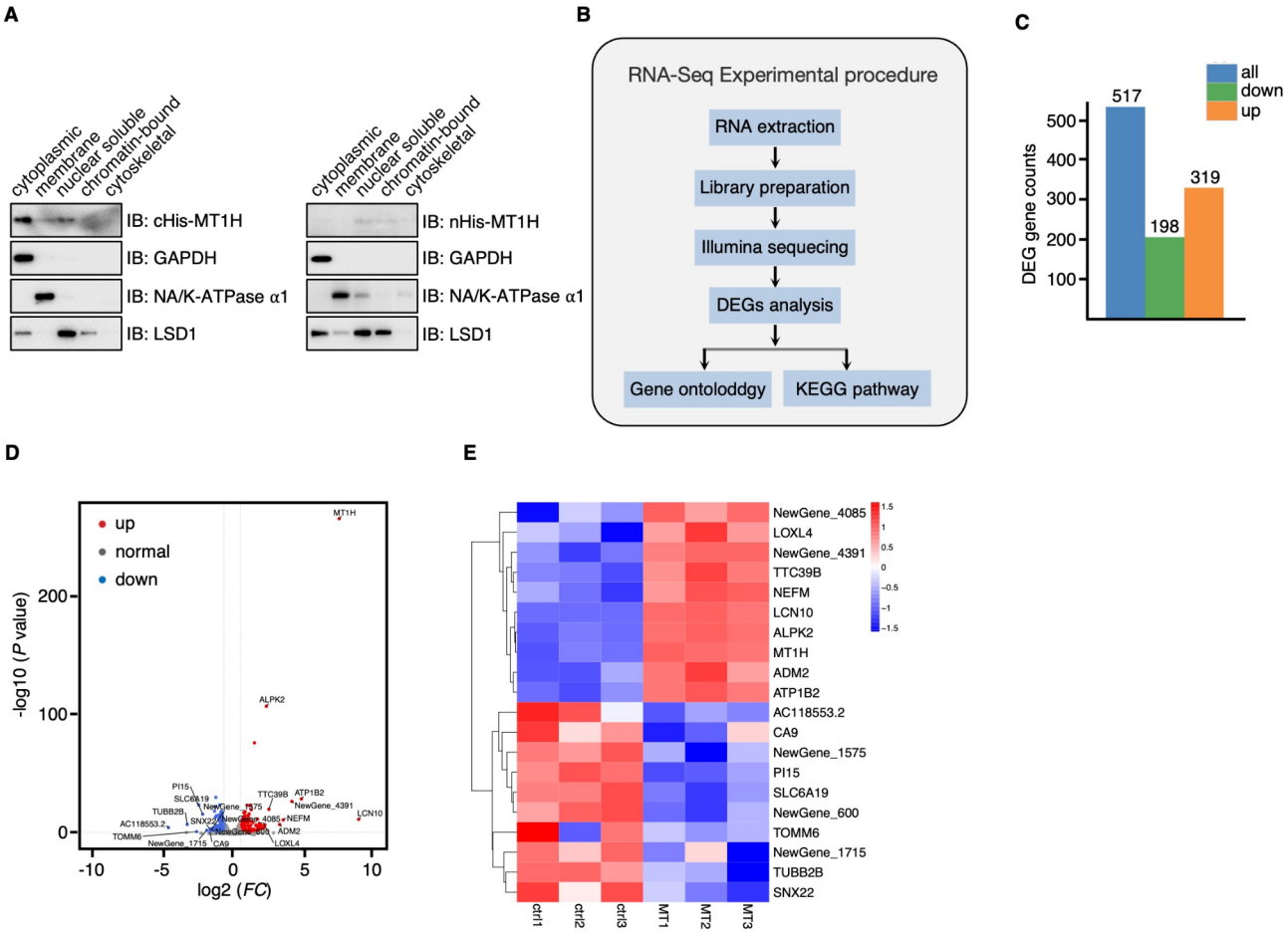

Fig. 4. RNA-seq identifies the DEGs regulated by MT1H. (A) Subcellular Fractionation. SGC-7901 cells transfected with MT1H were fractionated using Thermo Fisher Subcellular Fractionation Kit and immunoblotted with indicated antibodies. The proteins with clear subcellular distribution, including GAPDH, NA/K-ATPase α1, and LSD1, were used as fractionation indicators. 10% WCL was included as input control. (B) Experimental procedure of RNA-Seq analysis. (C) Bar plot of MT1H-DEGs. To quantify gene expression levels, expression levels were estimated as fragments per kilobase of transcript per million fragments mapped. Differential expression analysis of two conditions/groups was performed via DESeq2 (Version 1.30.1). The resulting *P* values were adjusted via Benjamini and Hochberg's approach for controlling the false discovery rate. Genes with an adjusted *P* value < 0.01 and a fold change ≥ 2 were considered differentially expressed. Blue represents all differentially expressed genes. Orange represents upregulated genes. Green represents downregulated genes. (D) MT1H-DEGs were shown in the volcano plot. Each point in the volcano plot represents a gene, with the x-axis representing the logarithmic value of the fold change in gene expression between two groups, and the y-axis representing the negative logarithmic value of the statistical significance of gene expression changes. The larger the absolute value on the x-axis, the greater the difference in expression levels between the two samples; the larger the value on the y-axis, the more significant the differential expression, and the more reliable the selected differentially expressed genes. The blue points in the plot represent downregulated differentially expressed genes, the red points represent upregulated differentially expressed genes, and the gray points represent non-differentially expressed genes. The top ten downregulated and upregulated MT1H-DEGs were annotated. (E) Heat map of top ten downregulated and upregulated MT1H-DEGs. Data conversion with Z-score normalization and archival Clustering were performed to ensure effective comparison and visualization of data between different samples or genes. The x-axis represents the sample names and the clustering results of the samples, while the y-axis represents the differentially expressed genes and the clustering results of the genes. Each column in the graph represents a different sample, and each row represents a different gene. The color represents the expression level of the gene in the sample (log10).

Methods

Data reporting

No statistical methods were used to predetermine the sample size. The experiments were not randomized. Investigators were not blinded for allocation during the experiments or outcome assessment.

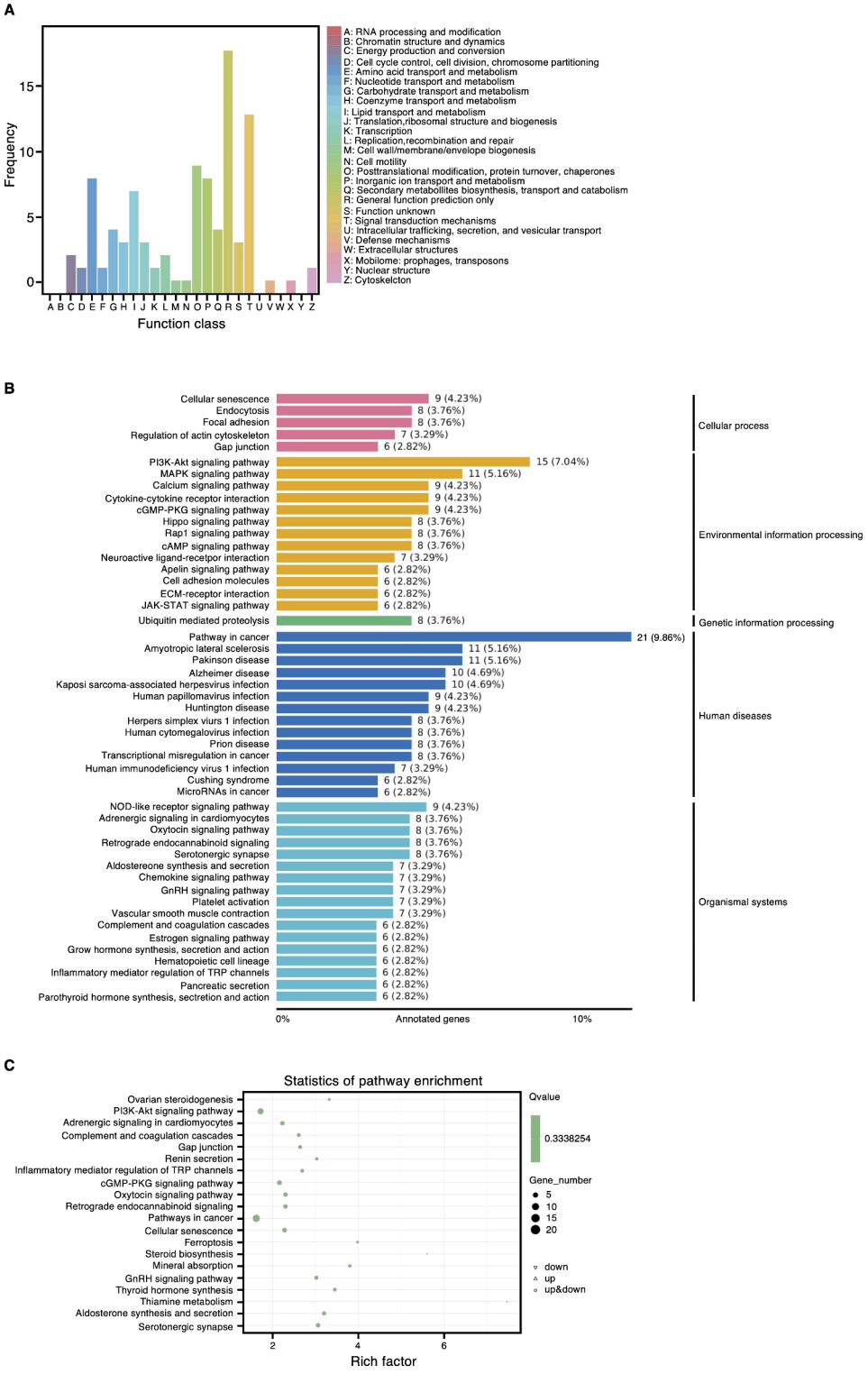

Ethics and consent to participate declarations

For the animal study, all methods were reviewed and approved by the Laboratory Animal Platform of Zhengzhou University (ZZU-LAC20240802[08]). All methods were carried out in accordance with relevant guidelines and regulations at Zhengzhou University. All methods are reported in accordance with ARRIVE guidelines. No human samples were used in this study.

Cell lines

The human immortalized gastric epithelial cell line GES-1, the human embryonic kidney epithelial cell line HEK293T, and the human gastric cancer cell lines AGS and SGC-7901 were purchased from the Chinese Academy of Sciences Shanghai Cell Bank (Shanghai, China). GES-1 and other cells were cultured in DMEM or RPMI 1640 (Gibco, Grand Island, NY, USA) media supplemented with 10% fetal bovine serum (Biological

◀**Fig. 5**. Gene functional annotation of MT1H-DEGs. For gene functional annotation, gene function was annotated via the following databases: Nr (NCBI nonredundant protein sequences); Pfam (Protein family); KOG/COG (Clusters of Orthologous Groups of proteins); Swiss-Prot (a manually annotated and reviewed protein sequence database); KO (KEGG Ortholog database); and GO (Gene Ontology). (A) COG Function Classification of MT1H-DEGs. KOG/COG (https://www.ncbi.nlm.nih.gov/COG/) is created by NCBI and primarily used for the homologous classification of gene products. MT1H-DEGs were classified according to COG Function Classification of Consensus Sequence. Shown is the bar plot of MT1H-DEGs. (B-C) KEGG pathway enrichment analysis of MT1H-DEGs. The KOBAS database and the clusterProfiler package (Version 4.4.4, http://www.bioconductor.org/packages/release/bioc/html/clusterProfiler.html) were used to test the statistical enrichment of MT1H-DEGs in KEGG pathways[55]. Shown are the bar plot (B) and bubble plot (C) of MT1H-DEGs. In C, the significance of a functional pathway is determined by the q-value, with a smaller q-value indicating a more significant pathway. The size of the dot represents the number of differentially expressed genes annotated in that pathway, and the color of the dot represents the q-value from the hypergeometric test. The dot closer to the top right corner has a higher reference value. (D-F) GO enrichment analysis of MT1H-DEGs. GO enrichment analysis was implemented via the clusterProfiler package (Version 4.4.4)-based Wallenius noncentral hypergeometric distribution, which can adjust for gene length bias in DEGs. MT1H-DEGs were enriched for molecular function (D), biological process (E), and cellular component (F) which was shown as bar plot (left panel) and bubble plot (right panel). In a bubble plot, the significance of a functional pathway is determined by the q-value, with a smaller q-value indicating a more significant pathway. The size of the dot represents the number of differentially expressed genes annotated in that pathway, and the color of the dot represents the q-value from the hypergeometric test. Rich factor refers to the ratio of the proportion of DEGs annotated to a specific pathway to the proportion of all genes annotated to that pathway. The greater the rich factor is, the more significant the enrichment level of DEGs in that pathway. The dot closer to the top right corner has a higher reference value.

Industries, Beit Haemek, Israel) and 5% CO_2 in a 37 °C humidified incubator for cultivation. All the cells were cultured in clean and free medium from Mycoplasma or other infections.

Western blotting

The cells were lysed in 150 µL of RIPA buffer (Gibco). The protein samples were subjected to SDS-PAGE and transferred to a polyvinylidene fluoride (PVDF) membrane. The membrane was blocked with 5% nonfat milk for 1 h, followed by incubation with primary antibody (overnight at 4 °C) and secondary antibody (1 h at room temperature). The ECL (Thermo Fisher Scientific) mixture was added to the membrane, and the images were visualized, adjusted, and captured with the Bio-Rad ChemiDoc™ XRS + system (Bio-Rad, Hercules, CA, USA).

Antibodies and reagents

For immunoblotting, LSD1 (2184), NF-κB p65 (8242T), RelB (4922T), Erk1/2 (9102), p-Erk1/2 (Thr202/Tyr204) (C4370S), and the Human Reactive Cell Death and Autophagy Antibody Sampler Kit (42867) were purchased from Cell Signaling Technology. Anti-Flag (F1804) and anti-HA (H6908) antibodies were obtained from Sigma–Aldrich. Anti-Na+/K + ATPase α1 mouse (PTM-5533) was purchased from PTM Biolabs. Anti-His (66005-1), anti-GAPDH (600041-Ig), anti-mTOR (66888-1-Ig), anti-p-mTOR (67778-1-Ig) and anti-p53 (10442-1-AP) were purchased from Proteintech. Anti-β-actin (sc-47778) was purchased from Santa Cruz Biotechnology. β-catenin (ab2365) was purchased from Abcam.

Protease inhibitor (A32953), nuclear and cytoplasmic extraction kit (78833) and subcellular fractionation kit (78840) were purchased from Thermo Scientific. Phosphatase inhibitor (B15002) was purchased from Bimake. Annexin V-FITC/PI apoptosis kit (KGA107) was purchased from KeyGEN BioTECH. Cell cycle kit (C1052) was purchased from Beyotime BioTECH. Cisplatin (HY-17394) was purchased from MedChemExpress. ZnCl2 (Z112532), CuCl2 (C106775), and FeCl2 (I106504) were purchased from Aladdin.

Semi-quantitative polymerase chain reaction (semi-qPCR)

To screen the inducers of MT1H expression, the cells were treated with the following conditions: Dexa (10 nM, 100 nM; 4 h,8 h,16 h), cisplatin (10 µM, 50 µM; 24 h), ZnCl2 (25 µM, 50, 150µM), CuCl2 (1 µM, 10 µM, 100 µM) and FeCl2 (25µM, 50 µM, 150 µM; 24 h). TRIzol Reagent (15596018, Invitrogen) was used to extract the total RNA according to the manufacturer's instructions. 1 µg of total RNA was used to synthesize prepare for cDNA templates for Semi-qPCR via a ReverTra-Ace qPCR RT kit (FSQ-101, TOYOBO). The primers were designed via NCBI primer BLAST, and the sequences are listed in Extended Table 2. The conditions for the PCR were optimized to obtain specific bands of the target genes, including the optimal annealing temperature and number of PCR cycles. To analyze the PCR products, 10 µl of each PCR product was loaded onto agarose (containing ethidium bromide). A DNA ladder was used to indicate the size of the PCR product. A negative control was included to determine DNA contamination from other sources. The intensity of a specific band was compared between different samples to estimate the relative abundance of the target DNA.

Apoptosis analysis kit

Gastric cancer cells with logarithmic growth were inoculated into 6-well plates and cultured in a 37 °C constant-temperature carbon dioxide incubator for 3–7 days. The cell confluence was less than 90% at the time of detection. After the cell supernatant was collected, the adherent cells were digested with 0.25% trypsin without EDTA. The digestion was terminated with the corresponding cell supernatant, which was collected in a 1.5 mL EP tube.

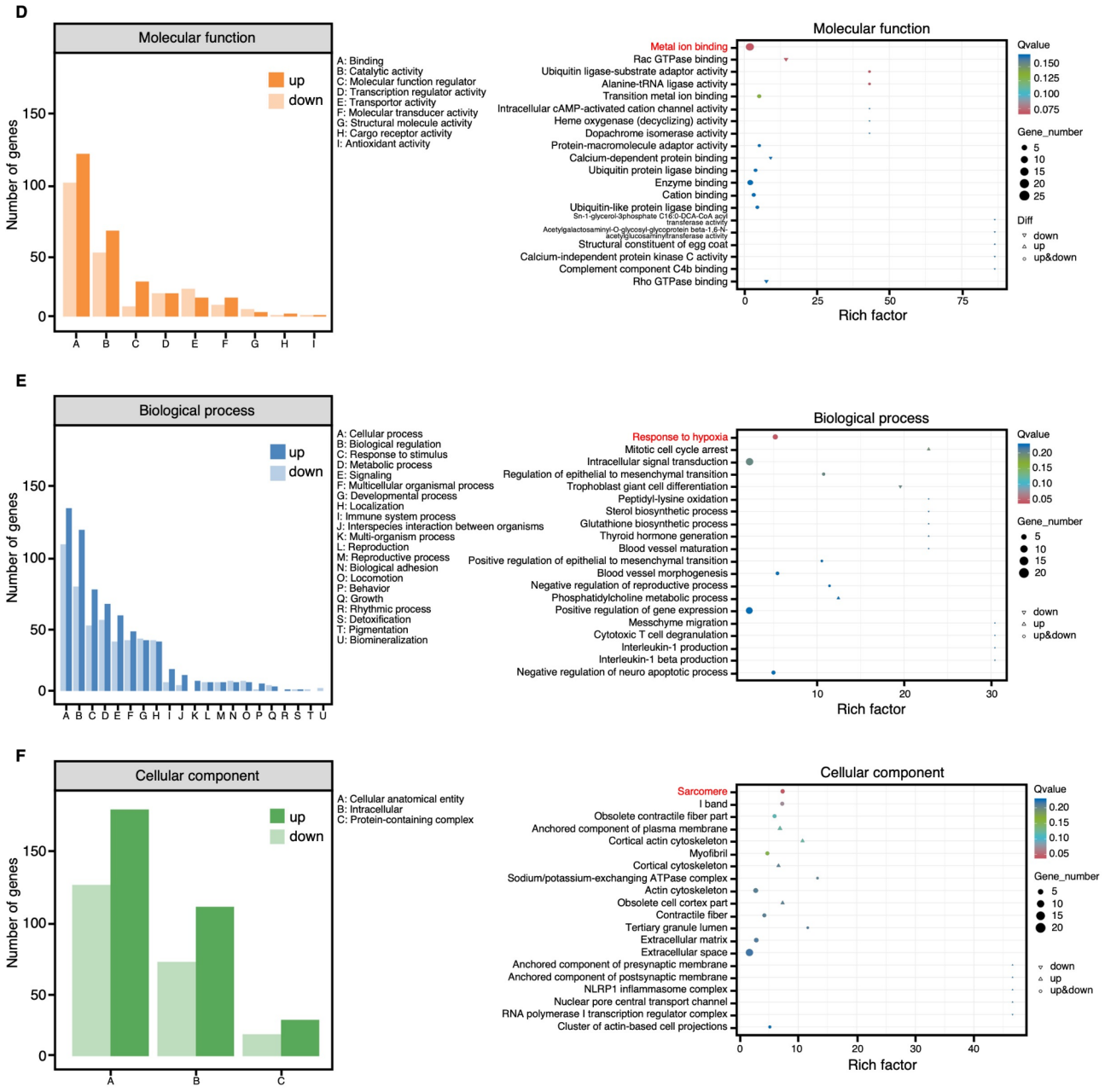

Figure 5. (continued)

Then, 500 mL of binding buffer, SrL Annexin V-FITC, and 5 NL Propidium were added to each tube, mixed with the mixture, and incubated at room temperature in the dark for 15 min. The excitation wavelength Ex = 488 nm was detected via flow cytometry, and the emission wavelength Em = 530 nm was used. Annexin V-FITC green fluorescence by FLI detection; PI red fluorescence (flowEx = 488 nm, Em ≥ 630 nm) was detected by FL3.

Cell cycle

10×10^5 cells were harvested and fixed in 1 mL of precooled 75% anhydrous ethanol overnight at -20 °C. After fixation, the cells were centrifuged, and 1 mL of PBS was added. Subsequently, 1 mL of DNA staining solution was added to each tube. The tubes were incubated for 30 min at room temperature and protected from light. DNA staining was then detected at a slower flow rate via FL3 on a flow cytometer.

Cell counting kit-8 (CCK-8)

The cells in the control group and the experimental group were cultured in good condition, digested with 0.25% pancreatic enzyme, and counted with a blood cell counting plate, and approximately 2000 cells/well were seeded in 96-well plates. Ten microliters of CC-K8 solution were added to each well after 7 days of culture. After 1 h, the OD values of the cells at 450 nm were measured via a microplate absorbance.

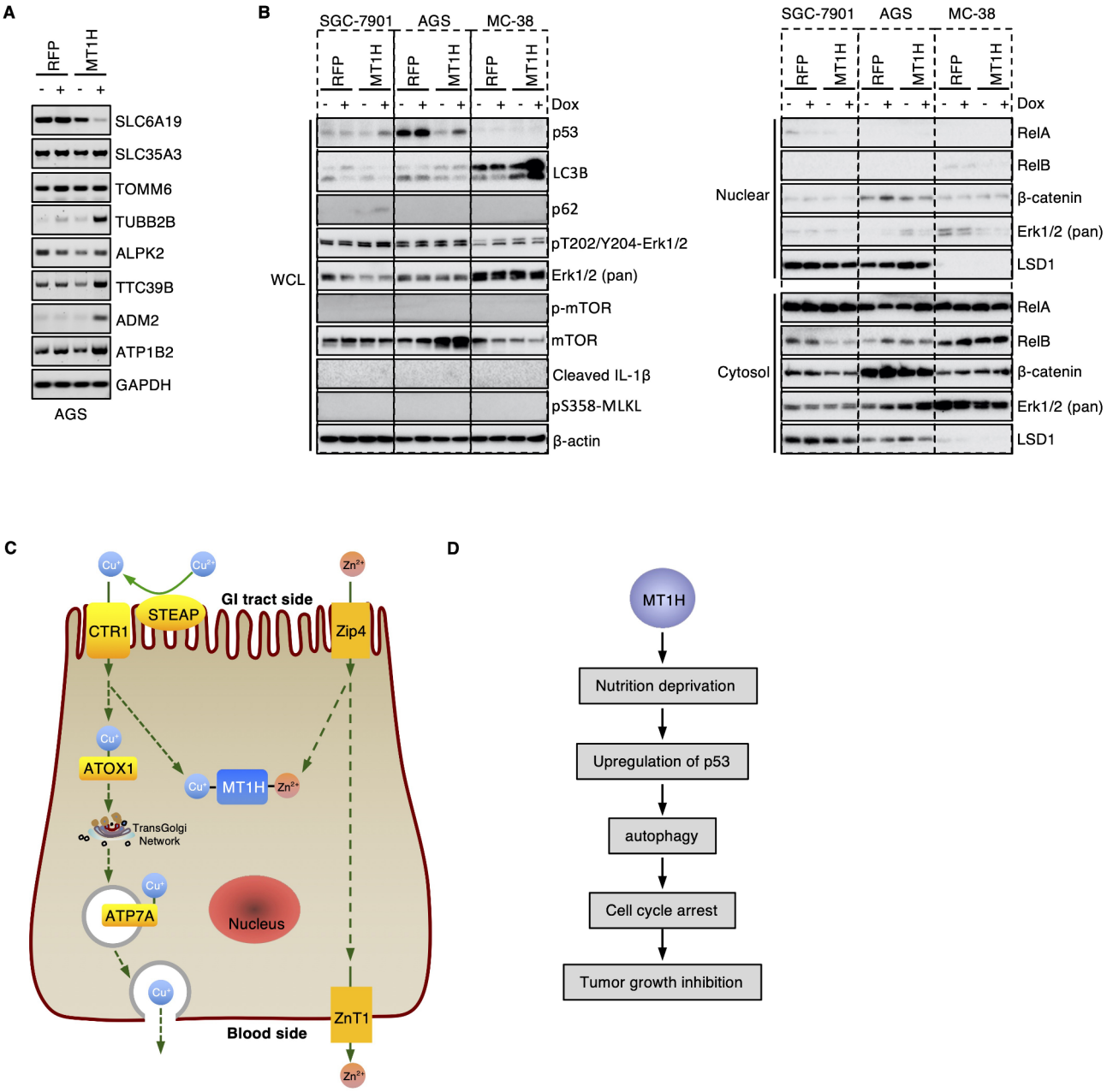

Fig. 6. MT1H induces p53-dependent autophagy via regulating the key genes in nutrient transportation. (A) Semi-qPCR to verify the downregulated or upregulated genes by MT1H in AGS cells. AGS-tetO-MT1H cells were treated with Dox (2 μg/ml) to induce the expression of ectopic MT1H. 24 h later, cells were harvested for total RNA extraction and reverse transcription followed by semi-qPCR. (B) The cells expressing tetO-MT1H were treated with Dox (2 μg/ml) to induce the expression of ectopic MT1H. 24 h later, cells were harvested for immunoblot analysis with indicated antibodies. NE-PER Nuclear and Cytoplasmic Extraction kit (Thermo) was used to fractionate cells into cytosol compartment and nuclear compartment. (C) MT1H biological functions by KEGG analysis. The participation in mineral absorption was predicted by KEGG-Pathway[55] (https://www.genome.jp/kegg/). (D) Illustrative diagram of MT1H biological functions in gastric cells. The information in the diagram is the combination of our current research and KEGG-Pathway.

RNA extraction cDNA library preparation for transcriptome sequencing

Total RNA was extracted according to the instruction manual of TRizol Reagent (Life Technologies, California, USA). The RNA concentration and purity were measured via a NanoDrop 2000 (Thermo Fisher Scientific, Wilmington, DE). RNA integrity was assessed via the RNA Nano 6000 Assay Kit of the Agilent Bioanalyzer 2100 system (Agilent Technologies, CA, USA). A total of 1 μg of RNA per sample was used as input material for the RNA sample preparations. The sequencing libraries were generated via the Hieff NGS Ultima Dual-mode mRNA Library Prep Kit for Illumina (Yeasen Biotechnology Co., Ltd., Shanghai) following the manufacturer's

A

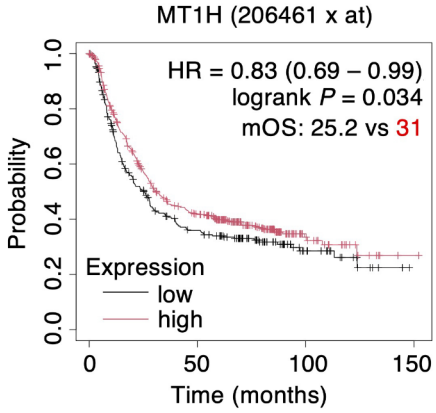

	Patient number at risk			
	0 mo.	50 mo.	100 mo.	150 mo.
MT1H low	304	90	20	0
MT1H high	571	208	28	1

B

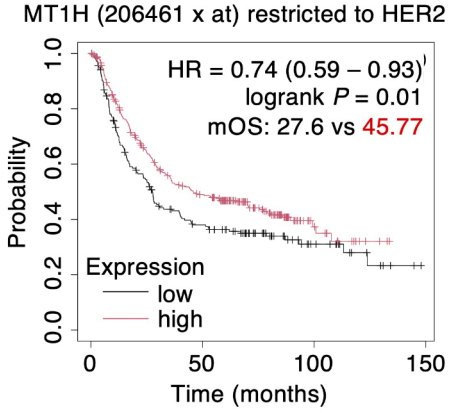

	Patient number at risk			
	0 mo.	50 mo.	100 mo.	150 mo.
MT1H low	205	66	16	0
MT1H high	327	139	17	0

C

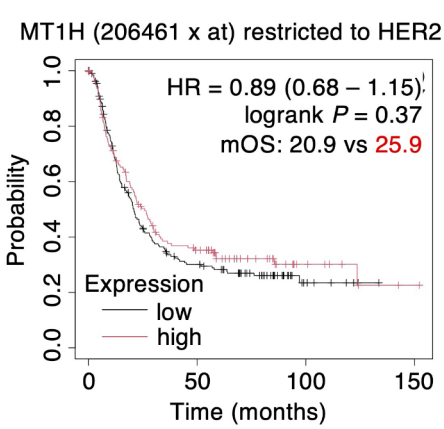

	Patient number at risk			
	0 mo.	50 mo.	100 mo.	150 mo.
MT1H low	202	51	7	0
MT1H high	141	42	8	1

Fig. 7. MT1H is a favorable biomarker for the prognosis of gastric cancer. (A) KM plotter analysis of MT1H based on gene-chip profiling in patients with gastric cancer ($n = 875$). Association between MT1H expression and patient survival was analyzed via the online tool Kaplan-Meier Plotter (https://kmplot.com/analysis/). The following dataset(s) were recruited for KM plotter analysis: GSE14210 ($n = 145$), GSE15459 ($n = 200$), GSE22377 ($n = 43$), GSE29272 ($n = 268$), GSE51105 ($n = 94$), GSE62254 ($n = 300$). Patients were split by median expression of MT1H. Survival of patients was determined by median OS. For array quality control, biased arrays were excluded. (B-C) Similar to (A), except that patients were firstly grouped into HER2 (-) (B) and HER2 (+) (C) according to the expression of HER2.

recommendations, and index codes were added to attribute the sequences to each sample. Briefly, mRNA was purified from total RNA using poly-T oligo-attached magnetic beads. First-strand cDNA was synthesized, and second-strand cDNA synthesis was subsequently performed. The remaining overhangs were converted into blunt ends using exonuclease/polymerase activities. After adenylation of the 3' ends of the DNA fragments, NEBNext Adaptor with a hairpin loop structure was ligated to prepare for hybridization. The library fragments were purified with the AMPure XP system (Beckman Coulter, Beverly, USA). Then, 3 µl of USER Enzyme (NEB,

A

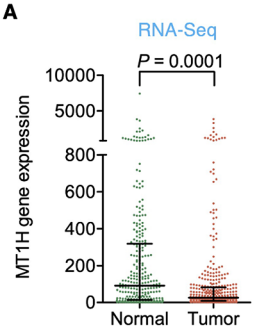

	Min	Q1	Med	Q3	Max	Upper whisker	N
Normal	0	14	91	316	7437	751	294
Tumor	0	9	26	82	3839	191	375

Mann_Whitney.p.	Fold.change..mean.	Fold.change..median.
1.19e-09	0.47	0.29

B

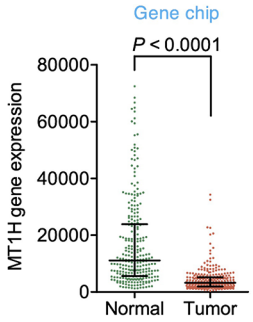

	Min	Q1	Med	Q3	Max	Upper whisker	N
Normal	1252	5620	11072	23844	72469	50859	273
Tumor	486	1932	3227	5127	34313	9540	273

Mann_Whitney.p.	Fold.change..mean.	Fold.change..median.
4.26e-35	0.26	0.29

C

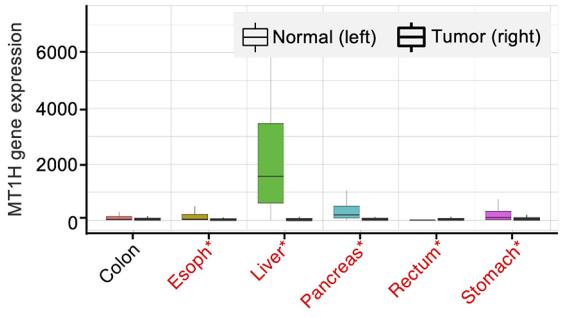

	Patient number					
	Colon	Esophagus	Liver	Pancreas	Rectum	Stomach
Normal	274	418	225	252	243	294
Tumor	469	161	371	177	166	375

D

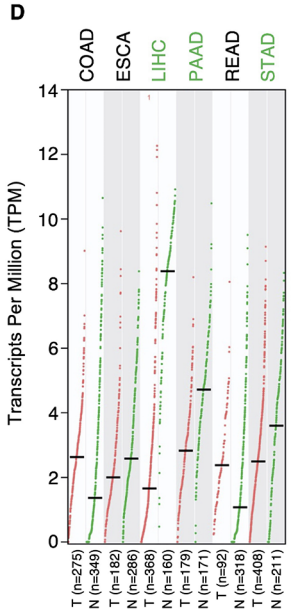

Fig. 8. MT1H is downregulated in gastric cancer. (A) MT1H expression in gastric cancer patients was assessed via TNM plot (https://tnmplot.com/analysis/). RNA-Seq data from normal and cancer tissues were used for TNM-plot analysis. Normal samples were obtained from non-cancerous patients and further pediatric tissues. (B) Similar to A, except that MT1H expression in gastric cancer patients was analyzed using Gene-Chip data. Only the paired tumor and adjacent normal tissues were included. (C) Similar to A, except that MT1H expression from cancers of the digestive system was analyzed. RNA-Seq data from normal and cancer tissues were used for TNM-plot analysis. Red*: Mann-Whitney $P < 0.05$ and expression > 10 in tumor or normal. (D) MT1H expression in patients with different cancers was assessed via GEPIA (http://gepia.cancer-pku.cn). For Gene Expression Profiling, the following parameters were used: ANOVA for Differential method; 1 for ILog2FCI cutoff; 0.05 for q-value cutoff. Matched Normal data were from Match TCGA normal and GTEx data. $\log_2(TPM + 1)$ for log-scale was used. Abbreviation: COAD, Colon adenocarcinoma; ESCA, Esophageal carcinoma; LIHC, Liver hepatocellular carcinoma; PAAD, Pancreatic adenocarcinoma; READ, Rectum adenocarcinoma; STAD, Stomach adenocarcinoma.

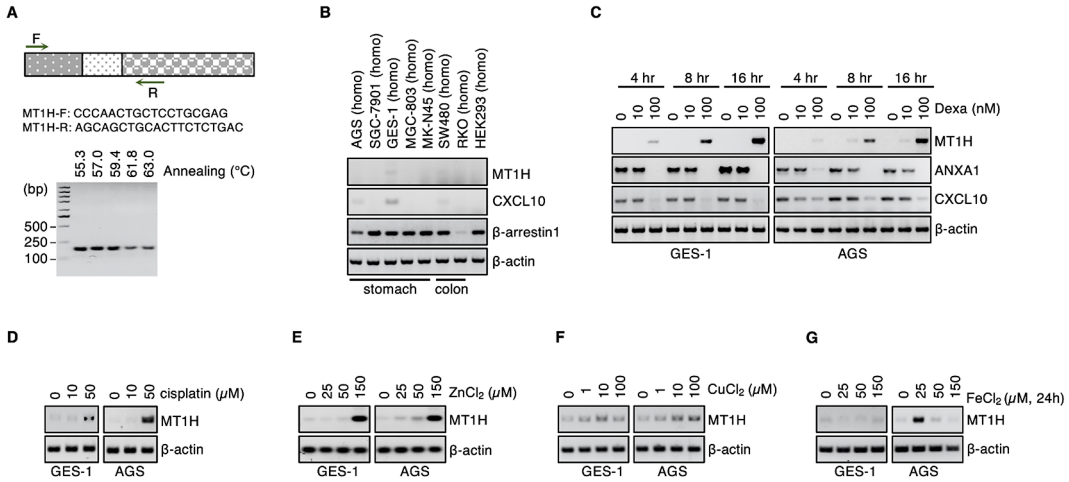

Fig. 9. MT1H has a glucocorticoid/metal-induced expression in gastric cancer cells. (A) Primer design of MT1H mRNA. Annealing temperature was optimized to get the specific PCR amplification of MT1H. 58℃ was used for the following PCR experiments. (B) MT1H mRNA expression was detected in different GI cancer cells via semi-qPCR. (C) MT1H has a glucocorticoid-induced expression in GI cancer cells. Cells were treated with different concentrations of Dexa (10, 100 nM) and harvested at different time points (4, 8, 16 h). (D-G) MT1H has a metal-induced expression in GI cancer cells. Cells were treated with different concentrations of cisplatin (10, 50 μM for 24 h) (D), $ZnCl_2$ (25, 50, 150 μM) (E), $CuCl_2$ (0, 1, 10, 100 μM) (F) and $FeCl_2$ (25, 50, 150 μM) (G). 24 h later, cells were harvested and subjected to semi-PCR assay.

USA) was used with size-selected, adaptor-ligated cDNA at 37 °C for 15 min, followed by 5 min at 95 °C before PCR. Then, PCR was performed with Phusion High-Fidelity DNA polymerase, universal PCR primers and Index (X) primers. Finally, the PCR products were purified (AMPure XP system), and library quality was assessed on an Agilent Bioanalyzer 2100 system.

RNA-seq and data processing

The libraries were sequenced on an Illumina NovaSeq platform to generate 150 bp paired-end reads according to the manufacturer's instructions. The raw reads were further processed with a bioinformatic pipeline, BMKCloud (www.biocloud.net), online platform. For quality control, raw data (raw reads) in fastq format were first processed through in-house Perl scripts. In this step, clean data (clean reads) were obtained by removing reads containing adapters, reads containing poly-N sequences and low-quality reads from the raw data. Moreover, the Q20, Q30, GC content and sequence duplication level of the clean data were calculated. All the downstream analyses were based on high-quality, clean data. Before the reads were mapped to the reference genome, the adaptor sequences and low-quality sequence reads were removed from the datasets. The raw sequences were transformed into clean reads after data processing. These clean reads were then mapped to the reference genome sequence. Only reads with a perfect match or one mismatch were further analyzed and annotated based on the reference genome. HISAT2 tools (Version 2.0.4) were used for mapping with the reference genome.

Bioinformatic analysis of RNA-seq data

For gene functional annotation, gene function was annotated via the following databases: Nr (NCBI nonredundant protein sequences); Pfam (Protein family); KOG/COG (Clusters of Orthologous Groups of proteins); Swiss-Prot (a manually annotated and reviewed protein sequence database); KO (KEGG Ortholog database); and GO (Gene Ontology). For quantification of gene expression levels, expression levels were estimated as fragments per kilobase of transcript per million fragments mapped. For differential expression analysis of the samples with biological replicates, differential expression analysis of two conditions/groups was performed via DESeq2 (Version 1.30.1). DESeq2 provides statistical routines for determining differential expression in digital gene expression data via a model based on the negative binomial distribution. The resulting *P* values were adjusted via Benjamini and Hochberg's approach for controlling the false discovery rate. Genes with an adjusted *P* value < 0.01 and a fold change ≥ 2 were considered differentially expressed. For differential expression analysis of the samples without biological replicates, differential expression analysis of two samples was performed via edgeR (Version 3.32.1). An FDR < 0.01 and a fold change ≥ 2 were set as the thresholds for significantly differential expression. Gene Ontology (GO) enrichment analysis of the differentially expressed genes (DEGs) was implemented via the clusterProfiler package (Version 4.4.4)-based Wallenius noncentral hypergeometric distribution, which can adjust for gene length bias in DEGs. For KEGG pathway enrichment analysis, we used the KOBAS database and the clusterProfiler package (Version 4.4.4) to test the statistical enrichment of DEGs in KEGG pathways[55].

Animal study

Ten BALB/c Nude male mice (18 ± 2 g) were purchased from Beijing Vital River Laboratory Animal Technology Co., Ltd. (Certificate No. SCXK2002-0003), approved by the Laboratory Animal Platform of Zhengzhou

University. Mice were kept at Room temperature 22 ± 1℃, controlled light (12 h light and dark cycle). 1×10^6 of either SGC7901-RFP or SGC7901-MT1H were subctaneously inoculated into the right flank of mice ($n = 5$ per group). The size of the tumor was monitored once every three days with calipers. Tumor volume (mm^3) is calculated via the "(W x W x L) / 2" formula, where L is the longest diameter and W is the shortest diameter. On day 25, the mice were sacrificed using cervical dislocation under anesthesia. Tumors were excised for weighing and photographing.

Statistical analysis

Student's t test was used to determine the differences between the two groups. Differences between tumor growth curves were compared by calculating the area under the curve values for each sample and then comparing different groups via Student's *t* test. The results are presented as the mean and standard error of the mean (SEM). Statistical significance was assigned to $P < 0.05$. Tumor-free survival and Kaplan–Meier analyses were performed via GraphPad Prism (Version 5.04) for Windows.

Reporting summary

Further information on the research design is available in the Research Reporting Summary linked to this paper.

Data availability

For the RNA-Seq, all data generated in this study were deposited in NCBI at Genbanks (PRJNA1202397), the SRA fastq files (SAMN45957133) are now undergoing the screening check on NCBI as well and will be released once they passed. The authors declare that all other data supporting the findings of this study are available in the paper and online supplementary material.

Received: 14 December 2024; Accepted: 19 February 2025
Published online: 18 March 2025

References

1. Klaassen, C. D., Liu, J. & Diwan, B. A. Metallothionein protection of cadmium toxicity. *Toxicol. Appl. Pharmacol.* **238**, 215–220. https://doi.org/10.1016/j.taap.2009.03.026 (2009).
2. Atrian, S. & Capdevila, M. Metallothionein-protein interactions. *Biomol. Concepts*. **4**, 143–160. https://doi.org/10.1515/bmc-2012-0049 (2013).
3. Kumari, M. V., Hiramatsu, M. & Ebadi, M. Free radical scavenging actions of Metallothionein isoforms I and II. *Free Radic Res.* **29**, 93–101. https://doi.org/10.1080/10715769800300111 (1998).
4. Thirumoorthy, N. et al. A review of Metallothionein isoforms and their role in pathophysiology. *World J. Surg. Oncol.* **9**, 54. https://doi.org/10.1186/1477-7819-9-54 (2011).
5. Takahashi, S. Molecular functions of Metallothionein and its role in hematological malignancies. *J. Hematol. Oncol.* **5**, 41. https://doi.org/10.1186/1756-8722-5-41 (2012).
6. Haq, F., Mahoney, M. & Koropatnick, J. Signaling events for Metallothionein induction. *Mutat. Res.* **533**, 211–226. https://doi.org/10.1016/j.mrfmmm.2003.07.014 (2003).
7. Artells, E., Palacios, O., Capdevila, M. & Atrian, S. In vivo-folded metal-metallothionein 3 complexes reveal the Cu-thionein rather than Zn-thionein character of this brain-specific mammalian Metallothionein. *FEBS J.* **281**, 1659–1678. https://doi.org/10.1111/febs.12731 (2014).
8. Quaife, C. J. et al. Induction of a new Metallothionein isoform (MT-IV) occurs during differentiation of stratified squamous epithelia. *Biochemistry* **33**, 7250–7259. https://doi.org/10.1021/bi00189a029 (1994).
9. Moleirinho, A. et al. Gains, losses and changes of function after gene duplication: study of the Metallothionein family. *PLoS One*. **6**, e18487. https://doi.org/10.1371/journal.pone.0018487 (2011).
10. Cherian, M. G., Jayasurya, A. & Bay, B. H. Metallothioneins in human tumors and potential roles in carcinogenesis. *Mutat. Res.* **533**, 201–209. https://doi.org/10.1016/j.mrfmmm.2003.07.013 (2003).
11. Bizon, A., Jedryczko, K. & Milnerowicz, H. The role of Metallothionein in oncogenesis and cancer treatment. *Postepy Hig Med. Dosw (Online)*. **71**, 98–109. https://doi.org/10.5604/01.3001.0010.3794 (2017).
12. Si, M. & Lang, J. The roles of Metallothioneins in carcinogenesis. *J. Hematol. Oncol.* **11**, 107. https://doi.org/10.1186/s13045-018-0645-x (2018).
13. Fu, J. et al. Metallothionein 1G functions as a tumor suppressor in thyroid cancer through modulating the PI3K/Akt signaling pathway. *BMC Cancer*. **13**, 462. https://doi.org/10.1186/1471-2407-13-462 (2013).
14. Ferrario, C. et al. Metallothionein 1G acts as an oncosupressor in papillary thyroid carcinoma. *Lab. Invest.* **88**, 474–481. https://doi.org/10.1038/labinvest.2008.17 (2008).
15. Han, Y. C. et al. Metallothionein 1 h tumour suppressor activity in prostate cancer is mediated by euchromatin methyltransferase 1. *J. Pathol.* **230**, 184–193. https://doi.org/10.1002/path.4169 (2013).
16. Wang, H., Guo, M., Wei, H. & Chen, Y. Targeting p53 pathways: mechanisms, structures, and advances in therapy. *Signal. Transduct. Target. Ther.* **8**, 92. https://doi.org/10.1038/s41392-023-01347-1 (2023).
17. Gao, M., Li, H. & Zhang, J. RB functions as a key regulator of senescence and tumor suppression. *Semin Cancer Biol.* **109**, 1–7. https://doi.org/10.1016/j.semcancer.2024.11.004 (2024).
18. Guo, Q. et al. NF-kappaB in biology and targeted therapy: new insights and translational implications. *Signal. Transduct. Target. Ther.* **9**, 53. https://doi.org/10.1038/s41392-024-01757-9 (2024).
19. Yu, H., Lin, L., Zhang, Z., Zhang, H. & Hu, H. Targeting NF-kappaB pathway for the therapy of diseases: mechanism and clinical study. *Signal. Transduct. Target. Ther.* **5**, 209. https://doi.org/10.1038/s41392-020-00312-6 (2020).
20. Hayat, R., Manzoor, M. & Hussain, A. Wnt signaling pathway: A comprehensive review. *Cell. Biol. Int.* **46**, 863–877. https://doi.org/10.1002/cbin.11797 (2022).
21. Zhang, Y. & Wang, X. Targeting the Wnt/beta-catenin signaling pathway in cancer. *J. Hematol. Oncol.* **13**, 165. https://doi.org/10.1186/s13045-020-00990-3 (2020).
22. Rim, E. Y., Clevers, H. & Nusse, R. The Wnt pathway: from signaling mechanisms to synthetic modulators. *Annu. Rev. Biochem.* **91**, 571–598. https://doi.org/10.1146/annurev-biochem-040320-103615 (2022).
23. Chen, A. et al. Zinc promotes cell proliferation via regulating metal-regulatory transcription factor 1 expression and transcriptional activity in pulmonary arterial hypertension. *Cell. Cycle*. **22**, 1284–1301. https://doi.org/10.1080/15384101.2023.2205209 (2023).
24. Maywald, M., Wessels, I. & Rink, L. Zinc signals and immunity. *Int. J. Mol. Sci.* **18** https://doi.org/10.3390/ijms18102222 (2017).

25. Wang, B., Fang, T. & Chen, H. Zinc and central nervous system disorders. *Nutrients* **15** https://doi.org/10.3390/nu15092140 (2023).
26. Gammoh, N. Z. & Rink, L. Zinc in infection and inflammation. *Nutrients* **9** https://doi.org/10.3390/nu9060624 (2017).
27. Kleta, R. et al. Mutations in SLC6A19, encoding B0AT1, cause hartnup disorder. *Nat. Genet.* **36**, 999–1002. https://doi.org/10.1038/ng1405 (2004).
28. Azmanov, D. N. et al. Further evidence for allelic heterogeneity in hartnup disorder. *Hum. Mutat.* **29**, 1217–1221. https://doi.org/10.1002/humu.20777 (2008).
29. Jewell, J. L., Russell, R. C. & Guan, K. L. Amino acid signalling upstream of mTOR. *Nat. Rev. Mol. Cell. Biol.* **14**, 133–139. https://doi.org/10.1038/nrm3522 (2013).
30. Filomeni, G., Desideri, E., Cardaci, S., Rotilio, G. & Ciriolo, M. R. Under the ROS… thiol network is the principal suspect for autophagy commitment. *Autophagy* **6**, 999–1005. https://doi.org/10.4161/auto.6.7.12754 (2010).
31. Hsieh, J. et al. TTC39B deficiency stabilizes LXR reducing both atherosclerosis and steatohepatitis. *Nature* **535**, 303–307. https://doi.org/10.1038/nature18628 (2016).
32. Roh, J., Chang, C. L., Bhalla, A., Klein, C. & Hsu, S. Y. Intermedin is a calcitonin/calcitonin gene-related peptide family peptide acting through the calcitonin receptor-like receptor/receptor activity-modifying protein receptor complexes. *J. Biol. Chem.* **279**, 7264–7274. https://doi.org/10.1074/jbc.M305332200 (2004).
33. Wei, P. et al. Intermedin attenuates myocardial infarction through activation of autophagy in a rat model of ischemic heart failure via both cAMP and MAPK/ERK1/2 pathways. *Int. J. Clin. Exp. Pathol.* **8**, 9836–9844 (2015).
34. Wang, M. et al. Effects of intermedin on autophagy in cerebral ischemia/reperfusion injury. *Neuropeptides* **68**, 15–21. https://doi.org/10.1016/j.npep.2017.10.004 (2018).
35. Zha, D. & Wu, X. Nutrient sensing, signaling transduction, and autophagy in podocyte injury: implications for kidney disease. *J. Nephrol.* **36**, 17–29. https://doi.org/10.1007/s40620-022-01365-2 (2023).
36. Glick, D., Barth, S. & Macleod, K. F. Autophagy: cellular and molecular mechanisms. *J. Pathol.* **221**, 3–12. https://doi.org/10.1002/path.2697 (2010).
37. Gyorffy, B. Integrated analysis of public datasets for the discovery and validation of survival-associated genes in solid tumors. *Innov. (Camb).* **5**, 100625. https://doi.org/10.1016/j.xinn.2024.100625 (2024).
38. Gyorffy, B. Transcriptome-level discovery of survival-associated biomarkers and therapy targets in non-small-cell lung cancer. *Br. J. Pharmacol.* **181**, 362–374. https://doi.org/10.1111/bph.16257 (2024).
39. Theocharis, S. E., Margeli, A. P., Klijanienko, J. T. & Kouraklis, G. P. Metallothionein expression in human neoplasia. *Histopathology* **45**, 103–118. https://doi.org/10.1111/j.1365-2559.2004.01922.x (2004).
40. Pedersen, M. O., Larsen, A., Stoltenberg, M. & Penkowa, M. The role of Metallothionein in oncogenesis and cancer prognosis. *Prog Histochem. Cytochem.* **44**, 29–64. https://doi.org/10.1016/j.proghi.2008.10.001 (2009).
41. Liu, Z. M. et al. Expression of functional Metallothionein isoforms in papillary thyroid cancer. *Mol. Cell. Endocrinol.* **302**, 92–98. https://doi.org/10.1016/j.mce.2008.12.017 (2009).
42. Bartha, A. & Gyorffy, B. TNMplot.com: A web tool for the comparison of gene expression in normal, tumor and metastatic tissues. *Int. J. Mol. Sci.* **22** https://doi.org/10.3390/ijms22052622 (2021).
43. Li, C., Tang, Z., Zhang, W., Ye, Z. & Liu, F. GEPIA2021: integrating multiple deconvolution-based analysis into GEPIA. *Nucleic Acids Res.* **49**, W242–W246. https://doi.org/10.1093/nar/gkab418 (2021).
44. Goff, J. P. Invited review: mineral absorption mechanisms, mineral interactions that affect acid-base and antioxidant status, and diet considerations to improve mineral status. *J. Dairy. Sci.* **101**, 2763–2813. https://doi.org/10.3168/jds.2017-13112 (2018).
45. Venturelli, S. et al. Minerals and cancer: overview of the possible diagnostic value. *Cancers (Basel).* 14. https://doi.org/10.3390/cancers14051256 (2022).
46. Margoshes, M. V. B. A cadmium protein from equine kidney cortex. *J. Chem. Soc.* **2** (1957).
47. Perez-Rafael, S. et al. Is MtnE, the fifth Drosophila metallothionein, functionally distinct from the other members of this polymorphic protein family? *Metallomics* **4**, 342–349 (2012). https://doi.org/10.1039/c2mt00182a
48. Zheng, Y. et al. Metallothionein 1H (MT1H) functions as a tumor suppressor in hepatocellular carcinoma through regulating Wnt/beta-catenin signaling pathway. *BMC Cancer*. **17**, 161. https://doi.org/10.1186/s12885-017-3139-2 (2017).
49. Hung, K. C. et al. The expression profile and prognostic significance of Metallothionein genes in colorectal Cancer. *Int. J. Mol. Sci.* **20** https://doi.org/10.3390/ijms20163849 (2019).
50. Liu, X. et al. Metallothionein 2A (MT2A) controls cell proliferation and liver metastasis by controlling the MST1/LATS2/YAP1 signaling pathway in colorectal cancer. *Cancer Cell. Int.* **22**, 205. https://doi.org/10.1186/s12935-022-02623-w (2022).
51. van Campagne, L. Evidence for a protective role of metallothionein-1 in focal cerebral ischemia. *Proc. Natl. Acad. Sci. U S A.* **96**, 12870–12875. https://doi.org/10.1073/pnas.96.22.12870 (1999).
52. Erickson, J. C., Hollopeter, G., Thomas, S. A., Froelick, G. J. & Palmiter, R. D. Disruption of the metallothionein-III gene in mice: analysis of brain zinc, behavior, and neuron vulnerability to metals, aging, and seizures. *J. Neurosci.* **17**, 1271–1281. https://doi.org/10.1523/JNEUROSCI.17-04-01271.1997 (1997).
53. Yin, L. et al. Novel germline mutation KMT2A G3131S confers genetic susceptibility to Familial myeloproliferative neoplasms. *Ann. Hematol.* **100**, 2229–2240. https://doi.org/10.1007/s00277-021-04562-4 (2021).
54. Li, J. et al. GNL3L exhibits pro-tumor activities via NF-kappaB pathway as a poor prognostic factor in acute myeloid leukemia. *J. Cancer.* **15**, 4072–4080. https://doi.org/10.7150/jca.95339 (2024).
55. Kanehisa, M., Furumichi, M., Sato, Y., Kawashima, M. & Ishiguro-Watanabe, M. KEGG for taxonomy-based analysis of pathways and genomes. *Nucleic Acids Res.* **51**, D587–D592. https://doi.org/10.1093/nar/gkac963 (2023).
56. Waterhouse, A. et al. SWISS-MODEL: homology modelling of protein structures and complexes. *Nucleic Acids Res.* **46**, W296–W303. https://doi.org/10.1093/nar/gky427 (2018).
57. Varadi, M. et al. AlphaFold protein structure database: massively expanding the structural coverage of protein-sequence space with high-accuracy models. *Nucleic Acids Res.* **50**, D439–D444. https://doi.org/10.1093/nar/gkab1061 (2022).
58. Jumper, J. et al. Highly accurate protein structure prediction with alphafold. *Nature* **596**, 583–589. https://doi.org/10.1038/s41586-021-03819-2 (2021).

Acknowledgements

Thanks to Xia Xue and Xiangdong Sun for revising the manuscript.

Author contributions

P.Z. and X.C. conceived the study and designed the experiment; Y.X. and GY.L. designed and performed the experiments; GG.L. J.X. provided technical assistance; X.C. analyzed the data and wrote the original manuscript; C.G. and T.Z. improved the overall language quality; M.L. and M.F. reviewed and edited the revised manuscript. All the authors have discussed the results and approved the final version of the manuscript for publication.

Declarations

Competing interests
The authors declare no competing interests.

Additional information
Supplementary Information The online version contains supplementary material available at https://doi.org/10.1038/s41598-025-91319-y.

Correspondence and requests for materials should be addressed to P.Z. or X.C.

Reprints and permissions information is available at www.nature.com/reprints.

Publisher's note Springer Nature remains neutral with regard to jurisdictional claims in published maps and institutional affiliations.